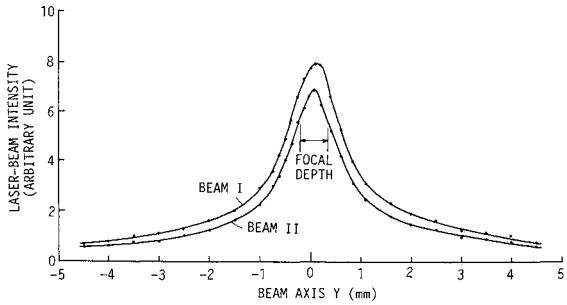

Fig. 3 Laser-beam intensity distribution along the beam axis. The focal depth is defined as the length of the measurement volume of the LTA along the beam.

peak amplitude indicates the beam intensity on the corresponding beam axis, and Fig. 2 clearly shows that beam I and beam II exhibit different intensities. The distance between the two peaks, however, represents the beam separation S, which is the critical parameter for velocity measurement with the LTA system. The accuracy with which this distance can be determined defines the accuracy of the overall measurement and is ultimately determined by the traversing mechanism precision. For this particular experiment, the traversing mechanism accuracy was ± 1 μm in the x axis and ± 5 μm in the y axis. These measurements are repeated at various beam-axis locations using an arbitrary origin, and peak amplitudes plotted against beam-axis location, as shown in Fig. 3. As indicated, each beam-intensity distribution is quite symmetrical about the peak position, and the peaks for each beam occur at exactly the same y location. This y location is the desired focal point for the LTA measurement. In the present application, the focal point is determined with an accuracy of about 0.1 mm in Fig. 3. If more accurate determination is desired, more data points near the peak in the distribution of Fig. 3 should be required, or rather, the focal point might be practically determined from the peak position on a spline joining the points of the distribution in Fig. 3.

Conclusions

A simple technique has been described for determining the exact focal point of a laser velocimeter, using only a hot-wire anemometer. To verify the proposed method, the focal-point separation of the two laser beams of an LTA system was measured. This example is only one potential application of the proposed technique, and others may include the laser Doppler velocimeter, or any laser measurement requiring exact knowledge of the focal-point location. Since hot-wire anemometers are extremely sensitive to thermal disturbances, the technique requires only modest laser beam power for the focal-point detection, as compared to that required for velocity measurement. Furthermore, since the squared bridge output of a constant-temperature anemometer indicates the mean value of the beam intensity intercepted by the hot-wire element, the method can be extended to evaluate other laser-beam parameters such as beam power, beam separation, beam diameter, relative beam intensity (e.g., between two laser beams), beam divergence, and cross-sectional beam-intensity distribution (Takagi[2]).

Acknowledgment

The author would like to express his sincere appreciation to Gregory A. Buck, Lighting Sciences, Inc., Scottsdale, Arizona, who kindly assisted with correcting the text.

References

[1]Schodl, R., "A Multi Colour Fiber Optic Laser Two Focus Velocimeter for Three-Dimensional Flow Analysis," AIAA Paper 88-3034, 1988.

[2]Takagi, S., "A Simple Method of Measuring Laser-Beam Properties Using a Hot-Wire Anemometer" (to be submitted).

New High Reynolds Number Mach 8 Capability

Eric R. Hedlund,* Craig W. Higgins,† Charles S. Rozanski,‡ Nancy F. Swinford,§ and John A. Hill§
Naval Surface Warfare Center, White Oak, Maryland 20910

Introduction

THE Naval Surface Warfare Center (NSWC) has an operational high Reynolds number Mach 8 leg in its Hypervelocity Wind Tunnel No. 9. This facility capability is unique and represents a benchmark in hypersonic aerodynamic ground testing. This Note highlights the facility development and summarizes its operational performance.

The NSWC Hypervelocity Wind Tunnel No. 9 is a blowdown facility that uses nitrogen as a working fluid. A test run is initiated by the rupture of two metal diaphragms that separate the high- and low-pressure sections of the wind tunnel. After initiation, the fixed volume of test gas, which is simultaneously heated and pressurized in the heater, expands through an axisymmetric contoured nozzle into the 5-ft-diam test section. Cold gas from pressurized storage vessels enters the heater base as the test gas exits, thereby maintaining a constant supply pressure throughout the wind-tunnel run. Run times, nominally 1 s in duration, are a function of the supply pressure and the fixed volume in the heater.

Tunnel 9 operates with interchangeable nozzles that expand the nitrogen to Mach numbers of 10, 14, and now 8. Reynolds numbers range from 0.5 to 20×10^6/ft at Mach 10 and 0.07 to 4×10^6/ft at Mach 14. Supply pressures range from 100 to 20,000 psia with supply temperatures up to 3400°R. Typical supply temperatures are chosen to operate the tunnel at a freestream temperature just above the nitrogen condensation temperature. More details on the operation of tunnel 9 can be found in Hill et al.,[1] Kavetsky,[2] Hedlund and Ragsdale,[3] and Ragsdale.[4]

Mach 8 Hardware Description

The Mach 8 development philosophy was to utilize as much existing hardware, including an auxiliary test cell, with no modifications to the high-pressure (heater and driver vessels) section of the tunnel. The existing Mach 10 heater assembly and thermal insulation package provided the supply gas to the Mach 8 nozzle. Figure 1 is a schematic layout of the tunnel components illustrating the hardware differences between the Mach 8 and 10 tunnel configurations. The Mach 8 nozzle is 20 ft long with an exit diameter of 33 in. Therefore, the facility operates in an open-jet fashion. More details on the design and fabrication of the hardware can be found in Hedlund et al.[5]

Calibration Tests

The Mach 8 calibration test included 10 flow survey runs and two verification data runs. The 10 flowfield survey runs were made with a 21-finger cruciform pitot rake. The rake

Received May 31, 1990; presented as Paper 90-1379 at the AIAA 16th Ground Testing Conference, Seattle, WA, June 18-20, 1990; revision received Sept. 3, 1991; accepted for publication Sept. 4, 1991.

*Chief Aerodynamicist, Aerodynamics Branch, K24. Senior Member AIAA.

†Mechanical Engineer, Aerodynamic Facilities Branch, K23.

‡Mechanical Design Group Leader, Aerodynamic Facilities Branch, K23.

§Aerospace Engineer, Aerodynamics Branch, K24. Member AIAA.

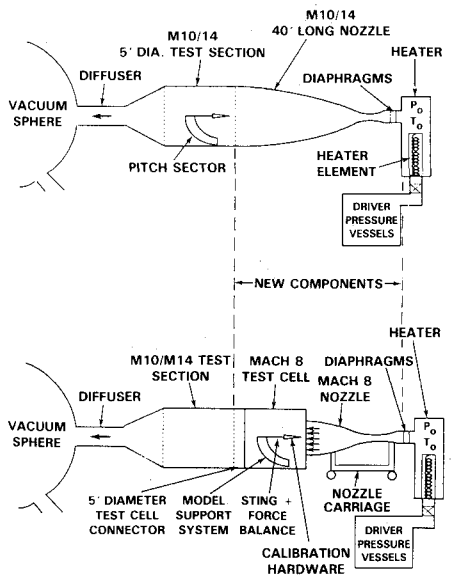

Fig. 1 Schematic of Mach 10/14 and Mach 8 tunnel hardware.

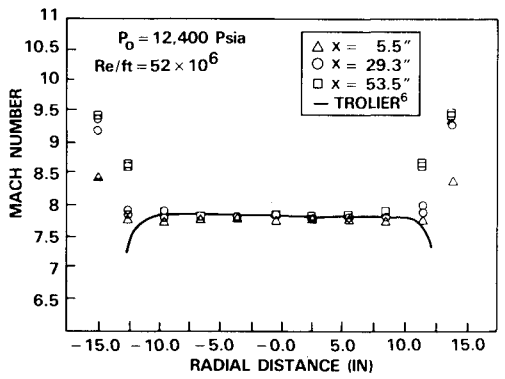

Fig. 2 Pitot rake calibration.

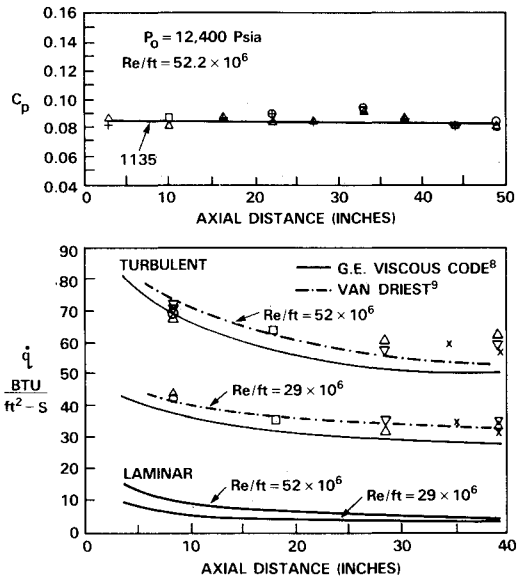

Fig. 3 Pressure coefficients and heat transfer rates on sharp cone.

measured 30.5 in. in width both horizontally and vertically. All pitots except the outermost pitot on each of the four legs were 3 in. apart (center to center). The four outer pitots were 2.5 in. from their neighboring probes. The rake was mounted on the sting with the probes oriented in the horizontal and vertical planes. The sting was moveable, which allowed the flow to be measured at various locations axially along the test section, thus establishing the boundaries of the uniform test core.

The two verification data runs were made with a sharp cone model at freestream Reynolds numbers of 29 and 52×10^6/ft. The model was an 11-deg half-angle aluminum cone with a stainless steel sharp nosetip, a base diameter of 20 in., and an overall length of 51.4 in. Surface pressure and heat transfer measurements were obtained at several axial and circumferential stations along the model. The cone was mounted at zero angle of attack, and the nosetip was positioned 1 in. upstream of the nozzle exit plane.

Calibration Data Analysis

Rake Data

Three runs were performed at the maximum supply conditions for the Mach 8 nozzle (nominal supply pressure of 12,400 psia and supply temperature of 1500°R). For these three runs, the rake was positioned at 53.5, 29.25, and 5.5 in., respectively, downstream from the nozzle exit plane. Mach number was calculated from the ratio of supply pressure to the pitot measurements. Real gas effects are accounted for in this calculation by the method described in Ref. 4.

Figure 2 is a plot of Mach number vs radial distance from the nozzle centerline for the three axial stations. The Mach number was 7.8 with a 24-in. uniform core diameter at the nozzle exit decreasing to a 16-in. uniform diameter at 53.5 in. downstream of the nozzle exit. Predictions performed by Trolier et al.[6] for the nozzle exit conditions agree well with the data in the inviscid core and the boundary-layer thickness. The Mach number uniformity was found to be ±0.5%. Mach number distributions at lower supply pressures had the same uniformity characteristics. Run time for a supply pressure of 12,400 psia was nominally 0.25 s.

Cone Data

Figure 3 shows the measured pressure coefficients C_p on the cone at several axial and circumferential stations at a Reynolds number of 52×10^6/ft. Also plotted is the inviscid pressure coefficient from the NACA 1135 report[7] for an 11-deg half-angle cone with an additional angular correction that accounts for the effect of the turbulent boundary-layer displacement thickness. The pressure distribution was expected to be fairly constant along the cone as inviscid theory predicts. For both runs, the average variability in the measured C_p values, both radially and circumferentially, was ±0.005 and the mean C_p value was approximately 4% higher than the theoretical inviscid value.

Figure 3 shows the measured heat transfer rate $\dot{q}$ at several axial and circumferential locations along the cone for freestream Reynolds numbers of 29 and 52×10^6/ft. The data were compared to two theoretical predictions, one generated by the General Electric (GE) viscous code[8] and the other from Van Driest's method.[9] The GE viscous code was run for a laminar and a turbulent boundary layer, whereas the prediction using Van Driest's method is for a turbulent boundary layer only. As can be seen in the plots, the data revealed a fully turbulent boundary layer for both Reynolds numbers. Van Driest's method predicted the heat transfer rates very well for both Reynolds numbers, whereas the GE viscous code underpredicted the data by 7–12%.

Summary

A new Mach 8 capability has been demonstrated in the NSWC Hypervelocity Tunnel No. 9. The following summarizes the new capabilities: Reynolds number = $17\text{–}52\times10^6$/ft, test time = 1.5–0.25 s, dynamic pressure = 28–85 psia, and test core (nozzle exit) = 24 in. Successful measurements of pressure and heat transfer have been obtained on a 20-in. base diameter sharp cone configuration that are in good agreement with theoretical predictions.

References

[1]Hill, J. A. F., Wardlaw, A. B., Jr., Pronchick, S. W., and Holmes, J. E., "Verification Tests in the Mach 14 Nozzle of the Hypervelocity Tunnel at NSWC (White Oak)," AIAA Paper 77-150, Jan. 1977.

[2]Kavetsky, R., "Mach 10 High Reynolds Number Development in the NSWC Hypervelocity Facility," Naval Surface Warfare Center, TR 83-526, White Oak, MD, June 1984.

[3]Hedlund, E. R., and Ragsdale, W. C., "Improvements in Low Reynolds Number Testing in the NSWC Hypervelocity Wind Tunnel #9," AIAA Paper 85-0226, Jan. 1985.

[4]Ragsdale, W. C., "Hypervelocity Wind Tunnel 9 Test Planning Guide," 2nd ed., Naval Surface Warfare Center, MP 88-200, White Oak, MD, Oct. 1989.

[5]Hedlund, E. R., Higgins, C. W., Rozanski, C. S., Fehring, N. P., and Krueger, D., "The New High Reynolds Number Mach 8 Capability in the NSWC Hypervelocity Wind Tunnel #9," AIAA Paper 90-1379, June 1990.

[6]Trolier, J. W., Sinha, N., and York, B., "Mach 8 Nozzle Design Verification, Science Applications International Corp., SAIC-88/1788, Fort Washington, PA, July 1988.

[7]Anon., "Report 1135: Equations, Tables, and Charts for Compressible Flow," NASA Ames Research Center, Moffett Field, CA, 1953.

[8]Hecht, A. M., Nestler, D. E., and Richbourg, D. H., "Application of a Three-Dimensional Viscous Computer Code to Reentry Vehicle Design," AIAA Paper 79-0306, Jan. 1979.

[9]Van Driest, E. R., "The Problem of Aerodynamic Heating," *Aeronautical Engineering Review*, Vol. 15, No. 10, Oct. 1956, pp. 26-41.

Optimum Design of a Composite Structure with Three Types of Manufacturing Constraints

Bo Ping Wang* and Daniel P. Costin†
University of Texas at Arlington, Arlington, Texas 76019

Introduction

THE application of composite materials to aircraft construction has provided the designer with increased flexibility. The orientation of plies can be tailored to provide aeroelastic performance unobtainable with an isotropic material. A tailored laminate is made up of plies of several orientations, usually 0, 45, −45, and 90 deg. The number of plies of each orientation varies from one zone to another on the plane of the laminate. Thus, a thick laminate with mainly 0-deg plies may form the root zone, and a thinner laminate with mainly ±45-deg plies may form the leading-edge zone. Often, however, the design flexibility allows extremely large variations of both the ply orientation percentage and laminate thickness. The large variations produce an uneven surface that is difficult to attach to other structures. The complexity of the laminate may increase manufacturing cost. Also, the large variations may cause stress concentrations that were not considered in the original analysis.

Manufacturing constraints have been applied to several types of designs. Toakley[1] used discrete design variables for steel structures, where only a finite number of standard beam cross sections were allowed. Schmit and Fleury[2] used discrete design variables for composite structures. The orientation thicknesses were constrained to be an integer multiple of the ply thickness. Upper- and lower-bound constraints on geometric design variables have been applied to stiffened composite panel designs.[3,4] These constraints controlled the thickness of the stiffener components and the width, height, and spacing of the stiffeners. Manufacturing constraints on aircraft wing skins have been applied by Petiau.[5] Petiau did not provide a mathematical description of the manufacturing constraints, but it is clear that constraints were placed on the thickness variation between adjacent design variables and on the proportion of plies in each direction.

The purpose of this Note is to mathematically define manufacturing constraints needed to control ply orientation percentage, thickness variation, and interleaving of plies from two adjacent zones. The constraints were implemented in the ASTROS optimization code and applied to the design of the simple wing structure described in the ASTROS applications manual.[6]

Mathematical Description of Constraints

To control the relative numbers of each orientation, an upper and lower bound must be placed on each orientation thickness $(t_n)_{\theta_i}$, where θ_i is the orientation angle, and n refers to a specific zone on the laminate, as shown in Fig. 1. The thickness of each layer is assumed to be a continuous design variable. The stacking sequence is not of concern since only the membrane properties are used in the finite element model.

The constraints control the thickness percentage of each orientation with respect to the total thickness. For example, the designer can specify that the thickness of each orientation must be greater than 10% of the total laminate thickness and less than 50% of the total laminate thickness. This type of constraint reduces the variation of the ply percentage across the laminate, but it also has structural benefits. This constraint type can be used to provide damage tolerance, bolted joint strength, and capability to carry unexpected loads. The mathematical expression of the constraint type is as follows:

$$(t_n)_{\theta_i} \le \frac{P_u}{100} \sum_{j=1}^{4} (t_n)_{\theta_j}, \qquad (t_n)_{\theta_i} \ge \frac{P_l}{100} \sum_{j=1}^{4} (t_n)_{\theta_j} \tag{1}$$

The parameter P_u is the upper-bound ply percentage, where $0 < P_u \le 100$. The parameter P_l is the lower-bound ply percentage, where $0 \le P_l < 100$. The sum in Eqs. (1) is the total laminate thickness for a specific zone. For use in ASTROS,

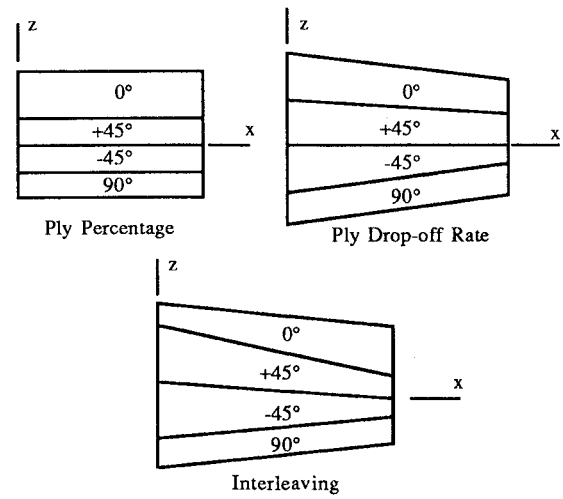

Fig. 1 Manufacturing constraints control ply orientation percentage, ply dropoff rate, and ply interleaving.

Received Feb. 4, 1991; presented as Paper 91-1133 at the AIAA/ASME/ASCE/AHS/ASC 32nd Structures, Structural Dynamics, and Materials Conference, Baltimore, MD, April 8-10, 1991; revision received Sept. 20, 1991; accepted for publication Sept. 23, 1991.

*Associate Professor, Department of Mechanical Engineering, Box 19023. Member AIAA.

†Research Assistant, Department of Mechanical Engineering, Box 19023. Member AIAA.